

Eutectic Microstructure and Thermoelectric Properties of Mg₂Sn

H.Y. CHEN^{1,2} and N. SAVVIDES¹

1.—CSIRO Materials Science and Engineering, Sydney, NSW 2070, Australia. 2.—e-mail: haiyan.chen@csiro.au

Ingots of undoped and Ag-doped Mg₂Sn were prepared from the melt using a rocking Bridgman furnace at different cooling rates: slow cooling (0.1 K/min), moderate cooling (1 K/min), and rapid quenching. The ingots show very different microstructure and thermoelectric properties. Slow-cooled ingots consist of large Mg₂Sn crystals with minor inclusions. Moderate-cooled ingots show significant variation in composition and microstructure, with Mg-rich material at the topmost section of the ingot and Sn-rich material at the bottom surface of the ingot. Rapid quenching results in ingots with finely dispersed Mg + Mg₂Sn eutectic microstructure in the form of lamellae 200 nm to 500 nm in thickness. Measurements of the Seebeck coefficient and electrical conductivity in the temperature range of $T = 80$ K to 700 K were carried out to establish correlations between the microstructure and the thermoelectric properties.

Key words: Eutectic microstructure, thermoelectric, Mg₂Sn

INTRODUCTION

The Mg₂X (X = Si, Ge, Sn) semiconductor compounds and their solid solutions have received attention as potential high-performance thermoelectric materials since the 1950s, and numerous investigations have been carried out regarding the electrical, optical, and thermal properties of Mg₂X.^{1–6} Recent work⁷ has shown that $ZT \approx 1.1$ can be achieved in Mg₂Si_{1-x}Sn_x solid solutions prepared by direct co-melting. Other preparation methods such as mechanical alloying,⁸ solid-state reaction,⁹ spark plasma sintering,¹⁰ and hot pressing^{11,12} have also been used.

There have been very few detailed reports, however, on the microstructure of Mg₂X compounds and their solid solutions. Due to the high vapor pressure and chemical reactivity of Mg, it is very difficult to obtain single-phase Mg₂X material, because unintentional inclusions can be introduced very easily by the above preparation methods. According to the effective-medium theory by Bergman and Levy,¹³ the thermoelectric figure of merit Z of a two- or multicomponent composite can never exceed the largest Z of each component of the composite.

However, as shown theoretically by Bergman and Fel¹⁴ and experimentally by Heremans and Jaworski,¹⁵ it may be possible to enhance the power factor if the components are a “high-quality thermoelectric” and a “benign metal.”

This paper is an extension of our earlier work^{16–18} to systematically investigate the crystal growth, microstructure, composition and doping, and thermoelectric properties of the Mg₂X compounds. Here we focus on the diverse microstructure of Mg₂Sn ingots grown from the melt at different cooling rates. The influence of the eutectic structure and secondary precipitates on the thermoelectric properties of pure and Ag-doped (*p*-type) Mg₂Sn are investigated and analyzed.

EXPERIMENTAL PROCEDURES

Five ingots of undoped and Ag-doped Mg₂Sn were prepared from the melt at different cooling rates. High-purity Mg (4 N), Sn (6 N), and Ag (3 N) were mixed with the desired atom ratio (Table I), then placed in a high-purity graphite or boron nitride crucible (with screwed cover) and sealed in a fused quartz ampoule under a mixture of Ar and H₂ gases at 0.8 MPa. The sealed quartz ampoule was suspended in the hottest zone of a vertical Bridgman tube furnace which has a sharp temperature

(Received July 9, 2009; accepted February 22, 2010;
published online March 13, 2010)

Table I. Sample ID, nominal composition, sample position in the ingot, and preparation conditions

Sample	Source Ingot and Sample Location	Nominal Composition		Cooling Rate (K/min)
		Mg:Sn	at.% Ag	
1	Ingot 1, middle/bottom	2.05:1	0	0.1
2	Ingot 2, middle/bottom	2.05:1	1	0.1
3	Ingot 3, bottom	2.06:1	0	1.0
4A	Ingot 4, bottom	2.06:1	1	1.0
4B	Ingot 4, middle/top	2.06:1	1	1.0
5	Ingot 5, middle/top	2.06:1	0	Quenched

gradient toward the bottom. When the temperature of the furnace reached 1073 K, the system was held there for 1 h, and the furnace was rocked from the vertical to the horizontal position once every 5 min. Following this procedure the tube furnace was held at the vertical position and the quartz ampoule was either lowered through the temperature gradient at a fixed cooling rate or was dropped into a container of water to quench the melt.

For the slow-cooled ingots (0.1 K/min) we used BN crucibles. During the lengthy processing a small amount of Mg vapor escaped via the BN screwed cover and reacted with the inner wall of the quartz ampoule, producing a thin layer of MgO + Si. For the ingots prepared at a moderate cooling rate (1 K/min) or by quenching we used graphite crucibles which are much cheaper to produce than ones made of BN. Although the processing time was shorter, the loss of Mg vapor during melting was quite apparent, and we compensated this loss by adding up to 3 at.% excess Mg to the charge prior to melting. Samples for characterization were cut from each ingot using a diamond saw. The sample ID, source ingot, nominal composition, and cooling rate are summarized in Table I.

The Mg-Sn binary phase diagram indicates that, when the melt is nonstoichiometric and not cooled at slow enough rates, the eutectic phase Mg₂Sn + Mg forms at 834 K if the melt is Mg rich, and the eutectic phase Mg₂Sn + Sn forms at 476 K if the melt is Sn rich.¹⁹ Our previous work has revealed that Mg₂Sn ingots grown at a slow cooling rate have nearly perfect stoichiometry except at the top end of the ingots, where minor amounts of free Sn were observed.¹⁸ By contrast, Mg₂Sn ingots grown at a moderate cooling rate show greater inhomogeneity in composition and microstructure, with the middle of the ingot being near-single-phase Mg₂Sn, the bottom surface being rich in Sn, and the top section containing regions of the Mg₂Sn + Mg eutectic structure.

The microstructure and thermoelectric properties of undoped and Ag-doped Mg₂Sn samples cut from the middle section of moderate-cooled ingots, which is near-single-phase Mg₂Sn with randomly dispersed Mg₂Sn + Mg eutectic structure, have

been discussed previously.¹⁶ Here, we focus on the influence of larger amounts of metallic inclusions of free Sn and Mg, and the Mg₂Sn + Mg eutectic phase, on the thermoelectric properties by studying samples that were cut from different sections of the ingots, as indicated in Table I.

The crystalline structure of the samples was investigated using a Philips X'Pert PRO x-ray diffractometer with Cu K_α radiation (wavelength $\lambda = 0.154$ nm). The microstructure was studied using a JEOL JSM-5400 field-emission scanning electron microscope (SEM) fitted with an energy-dispersive x-ray (EDX) spectrometer. Measurements of the Seebeck coefficient S and the electrical conductivity σ were done on samples about 2 mm × 3 mm × (12 mm to 15 mm) using a cryostat for $T = 80$ K to 300 K and a vacuum furnace above 300 K. The electrical conductivity σ was measured by the four-point probe technique, and the Seebeck coefficient was measured using chromel-constantan thermocouples and copper voltage probes. Each measurement was carried out for both rising and falling temperatures in the range of 80 K to 700 K.

RESULTS

Figure 1 shows typical x-ray diffraction data of coarse powder derived from ingots 1 to 5. The ingots grown at the slow cooling rates (1 and 2) are seen to be single-phase Mg₂Sn. Ingots 3 and 4, grown at moderate cooling rate, show additional diffraction peaks due to free Sn at the bottom section and free Mg at the top section of each ingot. Full pattern semiquantitative analysis using the X'Pert HighScore Plus software yields the content of excess Sn as 2 wt.% and 4 wt.% in sample 3 and 4A, respectively, and of excess Mg as 2 wt.% and 8 wt.% in samples 4B and 5, respectively.

Representative SEM micrographs of selected areas from each sample chosen for semiquantitative compositional analysis by EDX are shown in Fig. 2. The undoped sample 1, prepared at a slow cooling rate, is single-phase Mg₂Sn (Fig. 2a), while sample 2, doped with 1 at.% Ag, contains randomly dispersed particles of MgAg (Fig. 2b). Sample 3 (Fig. 2c) contains randomly distributed free Sn

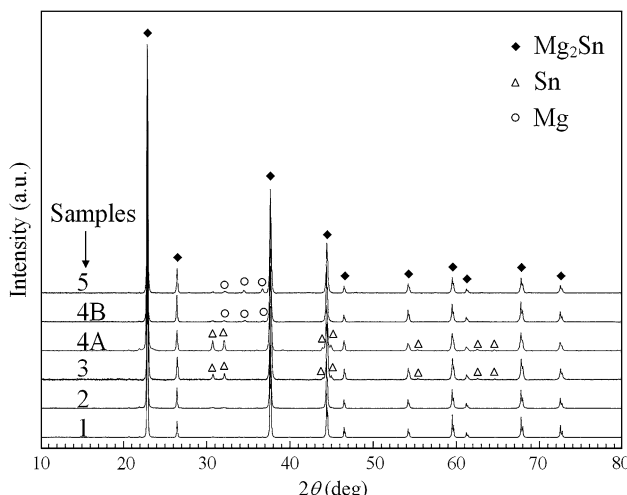


Fig. 1. X-ray diffraction spectra of crushed powder derived from ingots 1 to 5.

particles. The bottom section of ingot 4 (sample 4A) contains some free Sn, and at places small inclusions of a third phase (Fig. 2d); EDX analysis indicates that this third phase has the atom ratio Mg:Sn:Ag = 21:23:57. It has been reported that a Sn-Ag-Mg ternary alloy system has a eutectic temperature of 462 K where the transformation, liquid $\rightarrow \beta\text{-Sn} + \text{Mg}_2\text{Sn} + \text{Ag}_3\text{Sn}$ occurs.²⁰ Thus the third phase in Fig. 2d might be a Mg-rich Ag₃Sn alloy, formed by the dissolution of Mg atoms into the Ag₃Sn phase. The top section of the same ingot (sample 4B; Fig. 2e) contains large regions of free Mg that are in intimate contact with a fine eutectic structure identified by EDX to be Mg + AgMg₃. Figure 2f compares the EDX spectrum of the Mg₂Sn phase with the spectra of the three selected areas I, II, and III indicated on the SEM images and identified as MgAg, Mg-rich Ag₃Sn, and AgMg₃, respectively. The formation of these inclusions suggests that only part of the added silver is incorporated as dopant in the Mg₂Sn phase. Hall measurements from our earlier work¹⁸ show that, when the Ag content in the starting materials exceeds 0.25 at.%, the carrier concentration tends to saturate at $n \approx 6 \times 10^{19} \text{ cm}^{-3}$. Figure 2g and h shows the microstructure of the quenched sample 5. Here, the Mg₂Sn + Mg eutectic phase is dominant and it is interconnected, so that the pure Mg₂Sn phase occurs as large islands while the eutectic phase consists of domains of aligned lamellae of thickness 200 nm to 500 nm.

Figure 3 shows the temperature dependence of the Seebeck coefficient S from 80 K to 700 K for the five samples. Each sample was measured for both rising and falling temperature; the arrows indicate the direction of the temperature sweep. Regarding the undoped samples (Fig. 3a), samples 3 and 5 show some displacement in data after reaching the highest measurement temperature, which suggests

that there are measurable changes to the microstructure, composition, and/or the Ag-dopant distribution occurring during the high-temperature excursion. Subsequent cycling to the same high temperature did not yield further measurable changes in the Seebeck coefficient nor in the other transport properties. The $S(T)$ behavior of samples 1 and 3 is typical of undoped or lightly doped *p*-type Mg₂Sn semiconductors, where at low temperature the material is extrinsic and transits to thermally activated intrinsic conduction at higher temperatures.²¹ The presence of about 2 wt.% free Sn in sample 3 compared with the nominally stoichiometric sample 1 decreases the $S(T)$ peak. The $S(T)$ behavior of sample 5 is metal like, most likely due to the threading Mg lamellae of the interconnected Mg₂Sn + Mg eutectic structure. When ingots are doped with 1 at.% Ag, the samples show *p*-type $S(T)$ behavior that is characteristic of heavily doped semiconductors (Fig. 3b).

From the doped ingots we note that sample 4A (4 wt.% excess Sn and a small amount of Ag₃Sn) and sample 4B (2 wt.% excess Mg and minor Mg + AgMg₃ eutectic) have lower S values than sample 2 (single-phase Mg₂Sn with finely dispersed MgAg). Similarly, from the undoped ingots we note that sample 3 (single-phase Mg₂Sn with dispersed Sn particles) and sample 5 (metal-like interconnected Mg₂Sn + Mg eutectic phase with large Mg₂Sn islands) have lower S values in the extrinsic region than sample 1. These differences can be explained by the effective-medium theory of Bergman and Levy,¹³ according to which it is argued that the effective Seebeck coefficient of a two-component bulk composite must lie between the Seebeck coefficients of the two pure components. We also note that the Seebeck curves for samples 1, 2, and 4B are reproducible with temperature cycling while those of the Sn-rich samples 3, 4A, and 5 are displaced by a positive term during falling temperatures. We believe that this change in the Seebeck coefficient results from the loss of Sn (melting point 505 K) and possible recrystallization of the Sn phase. Indeed, small droplets of Sn were observed on the surface of sample 4A at the end of the measurements.

The temperature dependence of electrical conductivity σ for the undoped and Ag-doped samples is shown in Fig. 4a and b, respectively. It can be observed from Fig. 4a that, below 400 K, the electrical conductivity of sample 3 is higher than that of sample 1 but they tend to merge at higher temperatures with the onset of intrinsic conduction. Sample 5, which is metal like, shows much higher electrical conductivities over the entire temperature range as the Mg₂Sn + Mg eutectic structure dominates conduction. The three Ag-doped samples (Fig. 4b) have similar $\sigma(T)$ curves, but the Sn-rich sample 4A and the Mg-rich sample 4B show much higher values than the undoped sample 2. The $\sigma(T)$ curve of sample 4A at falling temperature differs from the curves $\sigma(T)$ at rising temperature. A small

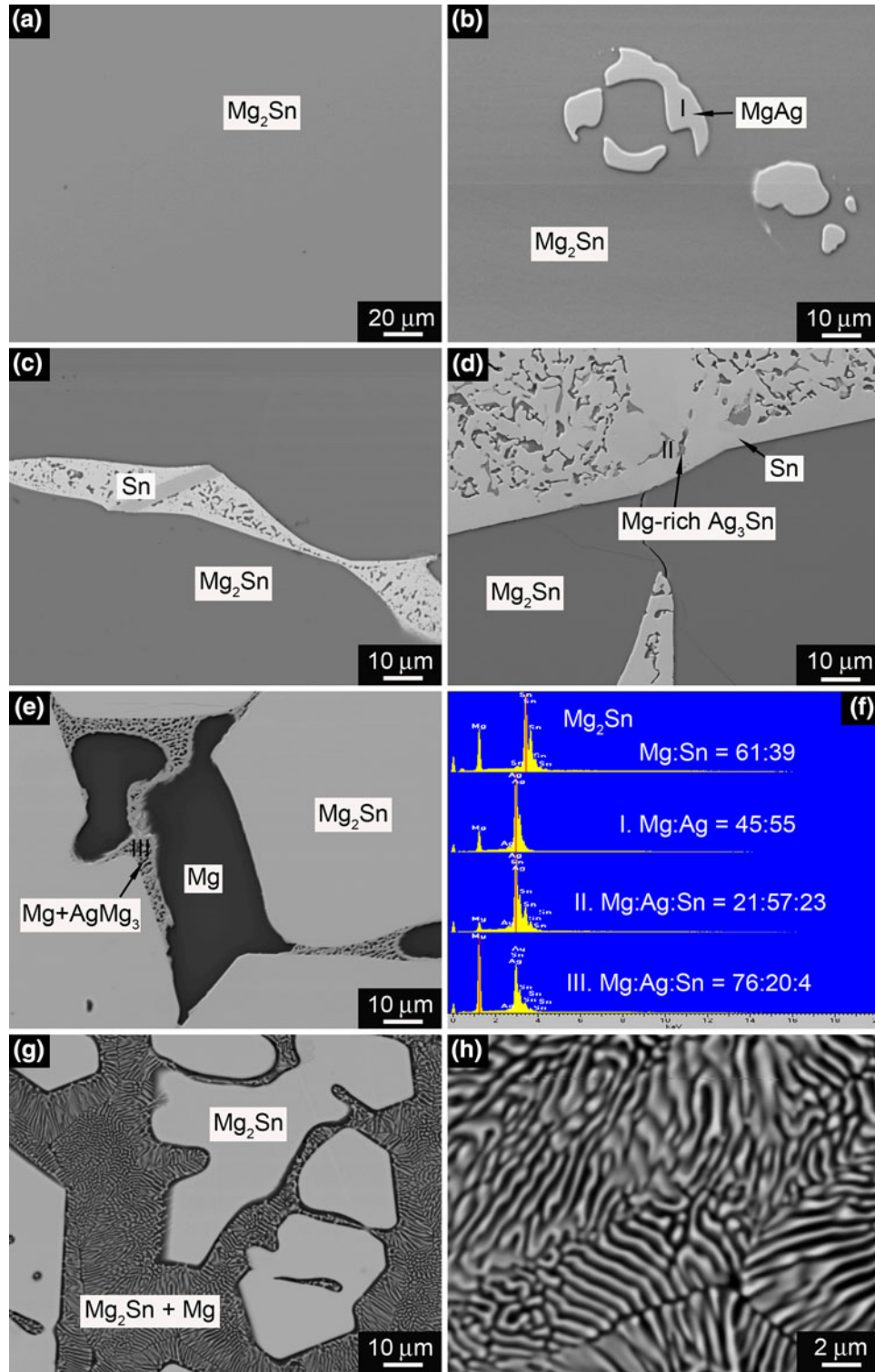


Fig. 2. SEM images and EDX spectra of Mg₂Sn ingots: (a) sample 1; (b) sample 2; (c) sample 3; (d) sample 4A; (e) sample 4B; (f) EDX spectrum of Mg₂Sn and selected areas I, II, and III indicated on the SEM images, and showing the material's composition in at.%; (g) and (h) sample 5.

difference is also seen in the Seebeck data (Fig. 3b), which suggests that, once the sample temperature exceeds the melting temperature of Sn, the initial interconnected free Sn that is embedded in the matrix begins to disperse and then recrystallize

more randomly and thus the sample conductivity decreases as the temperature is lowered.

The thermoelectric power factor, $P = \alpha^2\sigma$, calculated from the measured values of α and σ , is shown in Fig. 5. The undoped samples (1, 3, and 5)

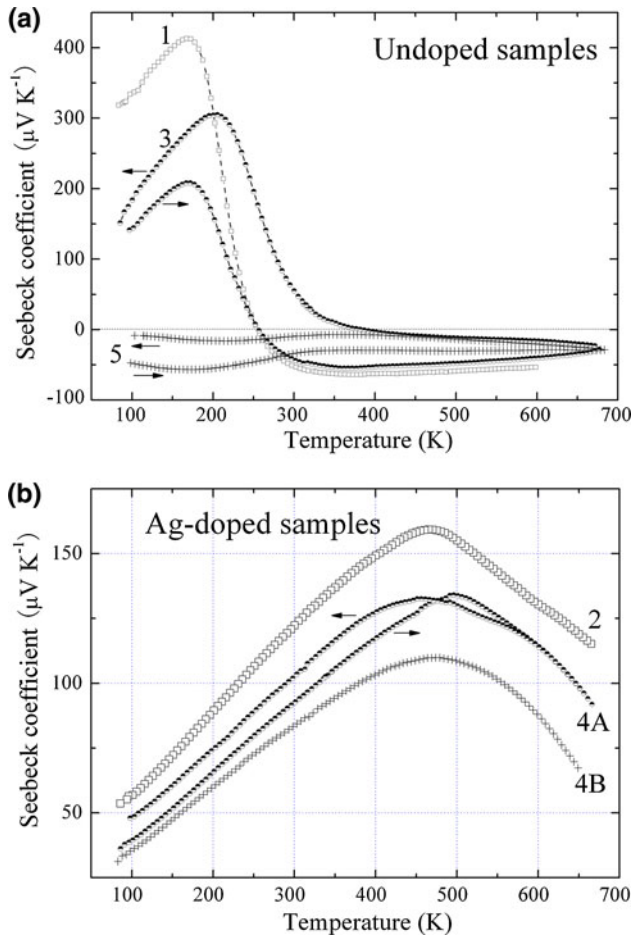


Fig. 3. Temperature dependence of the Seebeck coefficient of Mg_2Sn ingots: (a) undoped samples, and (b) Ag-doped samples. The arrows indicate the direction of the temperature sweep: → for rising temperature and ← for falling temperature.

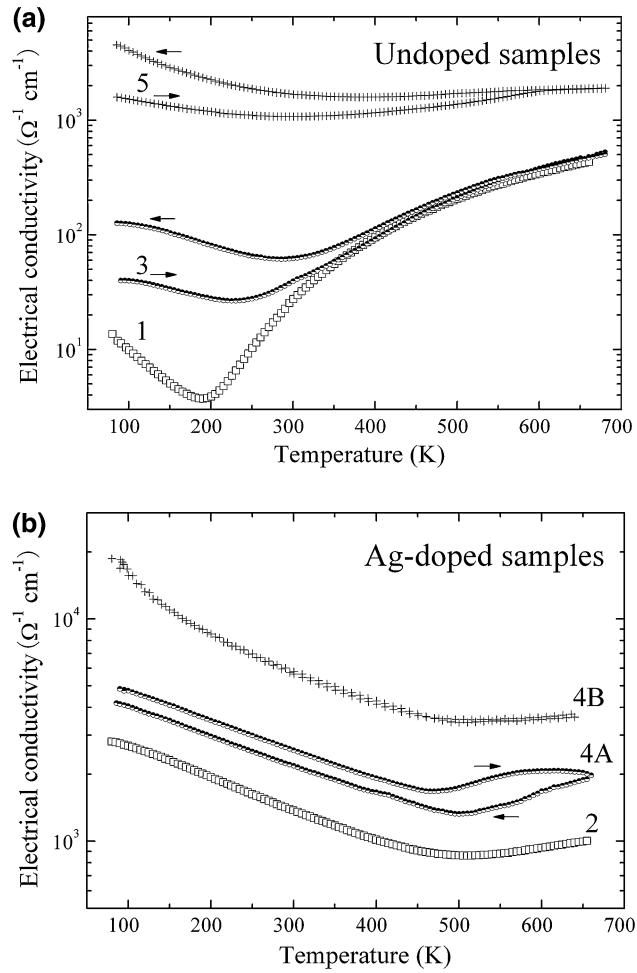


Fig. 4. Temperature dependence of the electrical conductivity of Mg_2Sn ingots: (a) undoped samples, and (b) Ag-doped samples.

have very low power factors, with sample 3 having a peak value of $0.75 \times 10^{-3} \text{ W/m/K}^2$ at 180 K. Although the Ag-doped samples (4A and 4B) contain small amounts of excess Sn or Mg, they have higher P values than sample 2 (which is also doped with the same Ag content), with sample 4B reaching a peak value of $4.5 \times 10^{-3} \text{ W/m/K}^2$ in a wide temperature range of 350 K to 600 K. This suggests that the increased electrical conductivity (Fig. 4b) due to the metal-like Mg inclusions (Fig. 2e) outweighs the effect of the lower Seebeck coefficient (Fig. 3b) and thus causes the observed enhancement of the power factor. Based on the thermal conductivity values presented in our companion paper²² and the values measured above 300 K,²³ $\kappa = 4.5 \text{ W/m/K}$ to 5 W/m/K at 400 K to 600 K for Mg_2Sn samples doped with 1 at.% Ag, we estimate $ZT_{\max} = 0.45$ for sample 4B.

CONCLUSIONS

Undoped and Ag-doped (*p*-type) ingots of the thermoelectric compound Mg_2Sn were prepared

using a rocking Bridgman furnace. The diverse microstructure of the Mg_2Sn ingots grown from the melt at different cooling rates (slow, fast, and quenched) and its influence on the thermoelectric properties were investigated and analyzed.

Slow-cooled (0.1 K/min) ingots are single-phase Mg_2Sn , while the ingots cooled at a faster rate (1 K/min) show significant variation in composition and microstructure, with Mg-rich material at the topmost section of the ingot and Sn-rich material at the bottom section of the ingot. Apart from its role as a *p*-type dopant, the addition of silver to the melt leads to the incorporation of minor inclusions of Ag_3Sn and AgMg_3 in the ingots. Rapid quenching of the melt results in ingots with dominant $\text{Mg}_2\text{Sn} + \text{Mg}$ eutectic phase with isolated Mg_2Sn material where the eutectic consists of regions of partly aligned lamellae, 200 nm to 500 nm in thickness.

Measurements of the thermoelectric properties from about 80 K to 700 K show that the presence of excess Sn or Mg decreases the absolute values of the Seebeck coefficient but causes the electrical conductivity to increase. The net effect of a small

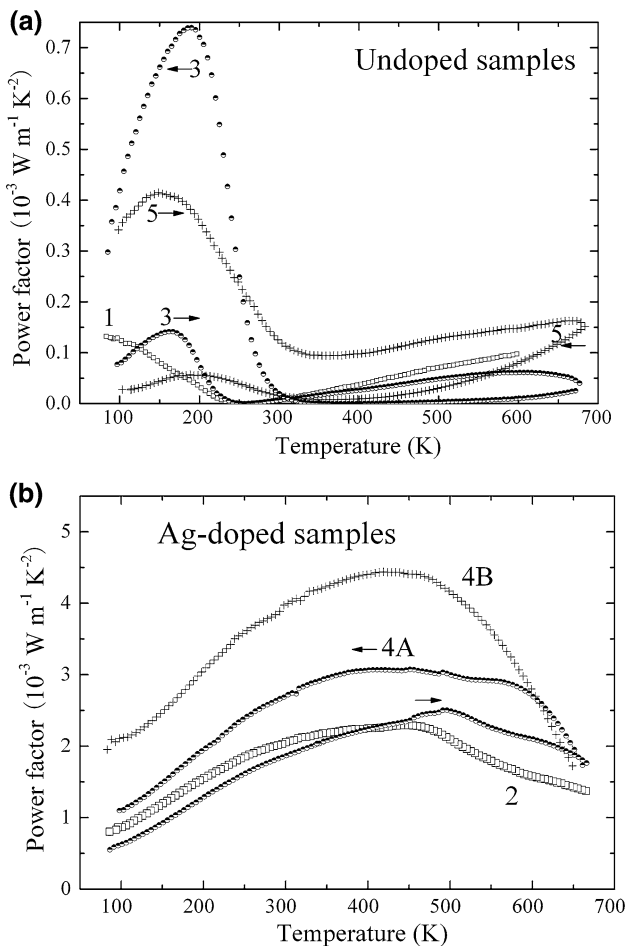


Fig. 5. Temperature dependence of the power factor: (a) undoped samples, and (b) Ag-doped samples.

amount of finely dispersed inclusions leads to enhancement of the power factor, while larger amounts of free Mg or Sn or Mg₂Sn + Mg eutectic can form interconnected microstructures which, while causing the electrical conductivity to increase, also lower the Seebeck coefficient and thus lead to a lower power factor. However, it is possible to disperse these coarse inclusions by powder metallurgy

followed by hot pressing to produce bulk material with nanoscale grain size and containing a large concentration of submicron inclusions of metal-like and semiconducting secondary phases which would be effective in scattering phonons,²⁴ i.e., decreasing the thermal conductivity, thus greatly enhancing the figure of merit.

REFERENCES

1. G. Busch and U. Winkler, *Helv. Phys. Acta* 26, 578 (1953).
2. R.G. Morris, R.D. Redin, and G.C. Danielson, *Phys. Rev.* 109, 1909 (1958).
3. R.D. Redin, R.G. Morris, and G.C. Danielson, *Phys. Rev.* 109, 1916 (1958).
4. R.J. Labotz and D.R. Mason, *J. Electrochem. Soc.* 110, 121 (1963).
5. J.J. Hauser, *Phys. Rev. B* 11, 3860 (1975).
6. Y. Noda, H. Kon, Y. Furukawa, I.A. Nishida, and K. Masumoto, *Mater. Trans. JIM* 33, 851 (1992).
7. V.K. Zaitsev, M.I. Fedorov, E.A. Gurieva, I.S. Eremin, P.P. Konstantinov, A.Y. Samunin, and M.V. Vedernikov, *Phys. Rev. B*, 74, 045207.1 (2006).
8. M. Riffel and J. Schilz, *Scr. Mater.* 32, 1951 (1995).
9. T. Aizawa, R. Song, and A. Yamamoto, *Mater. Trans. JIM* 46, 1490 (2005).
10. J. Tani and H. Kido, *Physica B* 364, 218 (2005).
11. G.S. Nolas, D. Wang, and M. Beekman, *Phys. Rev. B* 76, 235204 (2007).
12. Q. Zhang, J. He, T.J. Zhu, S.N. Zhang, X.B. Zhao, and T.M. Tritt, *Appl. Phys. Lett.* 93, 102109 (2008).
13. D.J. Bergman and O. Levy, *J. Appl. Phys.* 70, 6821 (1991).
14. D.J. Bergman and L.G. Fel, *J. Appl. Phys.* 85, 8205 (1999).
15. J.P. Heremans and C.M. Jaworski, *Appl. Phys. Lett.* 93, 122107 (2008).
16. H.Y. Chen and N. Savvides, *J. Electron. Mater.* 38, 1056 (2009).
17. C. Chuang, N. Savvides, and S. Li, *J. Electron. Mater.* 38, 1008 (2009).
18. H.Y. Chen and N. Savvides, *Mater. Res. Soc. Symp. Proc.* 1166, 153 (2009).
19. H. Okamoto, *Desk Handbook: Phase Diagrams for Binary Alloys* (Materials Park, OH: ASM International, 2000), p. 554.
20. P. Wu and K. Bai, U. S. patent US 6824039-B2 (2004).
21. V.K. Zaitsev and E.N. Nikitin, *Sov. Phys. Solid State* 12, 289 (1970).
22. N. Savvides and H.Y. Chen, *J. Electron. Mater.* accepted (2010). doi:10.1007/s11664-009-0978-x.
23. H.Y. Chen, N. Savvides, T. Dasgupta, C. Stiewe, and E. Mueller, *J. Chem. Phys.* (2010) (submitted).
24. N. Savvides and H.J. Goldsmid, *J. Phys. C* 13, 4657 (1980).